Biomaterials 100 (2016) 101–109

Contents lists available at ScienceDirect

Biomaterials

journal homepage: www.elsevier.com/locate/biomaterials

Re-assessing the enhanced permeability and retention effect in peripheral arterial disease using radiolabeled long circulating nanoparticles

Christopher G. England [a, 1], Hyung-Jun Im [b, c, 1], Liangzhu Feng [d], Feng Chen [b], Stephen A. Graves [a], Reinier Hernandez [a], Hakan Orbay [e], Cheng Xu [b], Steve Y. Cho [b], Robert J. Nickles [a], Zhuang Liu [d], Dong Soo Lee [c], Weibo Cai [a, b, f, *]

[a] Department of Medical Physics, University of Wisconsin – Madison, Madison, WI 53705, USA
[b] Department of Radiology, University of Wisconsin – Madison, WI 53705, USA
[c] Department of Molecular Medicine and Biopharmaceutical Sciences, Department of Nuclear Medicine, Seoul National University, Seoul 110-744, South Korea
[d] Jiangsu Key Laboratory for Carbon-Based Functional Materials & Devices Laboratory, Soochow University Suzhou, Jiangsu 215123, China
[e] Department of Surgery, University of California-Davis, Sacramento, CA 95817, USA
[f] University of Wisconsin Carbone Cancer Center, Madison, WI 53705, USA

ARTICLE INFO

Article history:
Received 12 January 2016
Received in revised form
8 May 2016
Accepted 17 May 2016
Available online 21 May 2016

Keywords:
Reduced graphene oxide (RGO)
Iron oxide nanoparticle (IONP)
Enhanced permeability and retention (EPR) effect
Hindlimb ischemia
Positron emission tomography (PET)
Photoacoustic imaging

ABSTRACT

As peripheral arterial disease (PAD) results in muscle ischemia and neovascularization, it has been claimed that nanoparticles can passively accumulate in ischemic tissues through the enhanced permeability and retention (EPR) effect. At this time, a quantitative evaluation of the passive targeting capabilities of nanoparticles has not been reported in PAD. Using a murine model of hindlimb ischemia, we quantitatively assessed the passive targeting capabilities of ^{64}Cu-labeled PEGylated reduced graphene oxide – iron oxide nanoparticles (^{64}Cu-RGO-IONP-PEG) through the EPR effect using positron emission tomography (PET) imaging. Serial laser Doppler imaging was performed to monitor changes in blood perfusion upon surgical induction of ischemia. Nanoparticle accumulation was assessed at 3, 10, and 17 days post-surgery and found to be highest at 3 days post-surgery, with the ischemic hindlimb displaying an accumulation of 14.7 ± 0.5% injected dose per gram (%ID/g). Accumulation of ^{64}Cu-RGO-IONP-PEG was lowest at 17 days post-surgery, with the ischemic hindlimb displaying only 5.1 ± 0.5%ID/g. Furthermore, nanoparticle accumulation was confirmed by photoacoustic imaging (PA). The combination of PET and serial Doppler imaging showed that nanoparticle accumulation in the ischemic hindlimb negatively correlated with blood perfusion. Thus, we quantitatively confirmed that ^{64}Cu-RGO-IONP-PEG passively accumulated in ischemic tissue via the EPR effect, which is reduced as the perfusion normalizes. As ^{64}Cu-RGO-IONP-PEG displayed substantial accumulation in the ischemic tissue, this nanoparticle platform may function as a future theranostic agent, providing both imaging and therapeutic applications.

1. Introduction

Development of multifaceted theranostic nanoparticles has become increasingly popular, as researchers strive to produce simplified strategies for disease treatment and imaging. In particular, reduced graphene oxide (RGO)-based nanocomposites are widely investigated for several imaging and therapeutic applications. Previously, we described the preparation and functionalization of RGO-nanoparticles for drug loading [1]. In addition to the therapeutic potential of RGO-based nanoparticles, this nanoplatform may function as a multimodality imaging agent. Specifically, RGO-iron oxide nanoparticles (RGO-IONPs) display physical and chemical characteristics suitable for multimodality imaging, including an NIR absorbance required for photoacoustic imaging,

* Corresponding author. Departments of Radiology and Medical Physics, University of Wisconsin – Madison, Room 7137, 1111 Highland Ave, Madison, WI 53705-2275, USA.
E-mail address: wcai@uwhealth.org (W. Cai).
[1] These authors contributed equally to this work.

http://dx.doi.org/10.1016/j.biomaterials.2016.05.018
0142-9612/

T2-relaxivity properties needed for magnetic resonance imaging (MRI), and RGO-IONPs may be easily functionalized for other imaging modalities. For example, Hong *et al.* utilized positron emission tomography (PET) to map the distribution of ^{64}Cu-labeled RGO in a murine breast cancer xenograft model [2].

Peripheral artery disease (PAD) is an ailment prevalent in the elderly that arises from arterial stenosis in the extremities, including legs and feet [3]. As the vasculature fails to provide vital oxygen to the tissues, patients experience slower healing times, intermittent claudication, and possible gangrene [4]. PAD has become a global health concern affecting approximately 12 million individuals in the United States alone [5]. Furthermore, people with PAD are at a higher risk of developing coronary artery disease and cerebrovascular disease in comparison to the normal population, both of which may lead to stroke or heart attack [6]. The most severe form of obstructive PAD, known as critical limb ischemia (CLI), is the leading cause of non-injury amputation [7]. Current treatments for CLI aim to normalize blood perfusion and include surgical intervention to bypass blocked arteries, proangiogenic growth factors, and anti-platelet medications [8]. Surgical intervention to treat PAD has several limitations. First, bypass surgery is an invasive surgery with serious adverse effects, such as heart attack, stroke or infection. Second, bypass surgery only targets the macrovascular system, so an immediate response may not be sufficient for CLI patients. To enhance the circulation through the microvascular system, proangiogenic growth factor treatment has been assessed and shown efficacy in preclinical studies [9,10]. However, proangiogenic growth factor treatment is limited by low delivery efficiency and systemic off-target effects and has failed to show benefits in several clinical trials [8]. In this regard, nanoparticle-based proangiogenic gene or growth factor delivery has been proposed. Multiple preclinical studies using nanoparticle-based growth factor treatment showed improvement of blood perfusion [11]. However, accumulation of nanoparticles has not been quantitatively assessed, even though the high accumulation of nanoparticle in the ischemic site is a prerequisite to overcome the limitation of conventional proangiogenic gene or growth factor treatment.

Monitoring the success of therapeutic intervention remains critical for improving patient survival, yet there are few reliable noninvasive imaging techniques for PAD patients. Duplex Doppler ultrasound imaging can evaluate the location and extent of the disease and arterial hemodynamics, yet the scans are time-consuming and calcification stenosis can limit the evaluation [12]. Besides Doppler imaging, magnetic resonance angiography (MRA) and computed tomography angiography (CTA) are two additional modalities utilized for noninvasive imaging of PAD [13]. MRA can effectively assess the location and degree of stenosis; yet is limited by high cost, motion artifacts, and decreased signal caused by metal clips or stents. While CTA is less sensitive than MRA, this imaging modality has fast acquisition times. Both CTA and MRA could cause renal toxicity in patients with renal insufficiency, which is a relatively common status in patients with PAD [14]. Nanoparticles have also been used to image PAD in preclinical studies. Previously, Kim *et al.* developed fluorescently-labeled PEGylated silica nanoparticles for optical imaging of PAD using the hindlimb ischemia model [15]. Similarly Zhang *et al.* investigated fluorescently-labeled gelatin nanoparticles for imaging of PAD [16]. Using optical imaging techniques, they showed a significant difference in nanoparticle uptake at 4 h and 24 h post-injection. Nanoparticle accumulation was highest in the ischemic hindlimb at 4 h and significantly decreased at 24 h. While optical imaging showed a statistically significant difference in fluorescence signal between the ischemic and non-ischemic hindlimb, optical imaging lacks the sensitivity and penetration depth needed for accurate quantification. The high sensitivity of PET is well suited for quantitative evaluation of serial responses to medical intervention in patients with PAD by providing information regarding physiological changes in response to various therapies; yet currently, there is no established PET tracer to image PAD [17]. Also, multimodality imaging of PAD will allow for simultaneous assessment of the anatomy and physiology of the disease, guiding physicians in developing patient-specific treatment protocols [12].

While passive targeting via the enhanced permeability and retention (EPR) effect has been extensively examined in solid tumors, few studies have examined this phenomenon in other disease models, including PAD [15,18]. Similar to solid tumors, several angiogenic factors are upregulated in ischemic tissue that may activate and mobilize endothelial cells to form new leaky vessels, resulting in EPR-attributed nanoparticle localization [15]. However, the degree and the time course of the EPR effect have not been evaluated quantitatively in PAD. The EPR effect of nanoparticles depends on several factors, including the stability and circulation half-life [19]. The long circulation half-life of PEGylated RGO-IONPs *in vivo* provides adequate time for the EPR effect to cause nanoparticle localization in the ischemic hindlimb. Additionally, RGO-IONPs have shown excellent theranostic properties for disease imaging and treatment, including its optical absorbance properties, ability to deliver large drug payloads, and passive targeting capabilities [1].

Herein, we investigated ^{64}Cu-RGO-IONP-PEG for the noninvasive multimodal imaging of PAD using a murine model of hindlimb ischemia. A surgical procedure recreated the conditions found in PAD patients, and as the ischemic hindlimb healed (15–20 days), blood flow was restored to normal in the diseased hindlimb [20]. At 3, 10, and 17 days post-surgery, mice received an intravenous injection of ^{64}Cu-RGO-IONP-PEG and imaged for 72 h with PET. We could observe and quantify the accumulation of nanoparticles in the ischemic hindlimb. Also, we found that fewer nanoparticles localized in the ischemic tissue as the vasculature normalized, which might be explained by the lessened EPR effect. Accumulation of ^{64}Cu-RGO-IONP-PEG in the ischemic hindlimb confirmed the influence of the EPR effect, while also showing that ^{64}Cu-RGO-IONP-PEG is a suitable nanoplatform for the noninvasive multimodality imaging of PAD.

2. Materials and methods

2.1. Synthesis and surface functionalization of RGO-IONP

Synthesis of RGO-IONP-PEG was previously reported [21]. RGO-IONP was synthesized using a modification of the Hammer method. Briefly, GO (20 mg), $FeCl_3 \cdot 6H_2O$ (270 mg), sodium acrylate (750 mg), and sodium acetate (750 mg) were dissolved in a mixture of ethylene glycol (0.5 mL) and diethylene glycol (9.5 mL). The solution was heated at 200 °C for 10 h and resulting RGO-IONP was washed with ethanol and deionized water. Synthesis of the RGO-IONP nanocomposites was accomplished through a hydrothermal reaction between the RGO and iron chloride hexahydrate. To ensure biocompatibility and increased blood circulation *in vivo*, RGO-IONP (1 mg) were functionalized with 10 mg of poly(maleicanhydride-alt-1-octadecene) (PEG) (Sigma-Aldrich, Madison, WI, USA). The solution was sonicated for 30 min and centrifuged at 4000 rpm for 5 min to remove unstable aggregates before the supernatant was washed through a 100-nm filter membrane to remove unbound PEG. On the RGO-IONP-PEG, we conjugated additional PEG for a longer circulation time and NOTA for radiolabeling. Before the addition of second PEG, nanoparticles were conjugated to p-SCN-Bn-NOTA (NOTA, Macrocyclics, Inc., Dallas, TX, USA) with 1:4 M ratio of the nanoparticle to the chelator. The pH of the solution was

adjusted to 9 and reacted overnight before desalting purification. 3 mg Malemide-PEG-SCM_{5K} (PEG) (Creative PEGWorks, Chapel Hill, NC, USA) was added to the nanoparticle solution (~0.5 mg) after NOTA conjugation. Finally, NOTA-RGO-IONP-PEG was obtained.

2.2. Characterization of NOTA-RGO-IONP

RGO-IONP nanocomposites underwent several instrumental tests to confirm their identity. The size of nanoparticles was measured by dynamic light scattering (DLS). The surface charge of RGO-IONP-PEG was examined using the ZetaSizer (Malvern, Worcestershire, UK). Atomic force microscopy (AFM) (Bruker BioScope Catalyst AFM, Middleton, WI, USA) was used to investigate the morphology of ^{64}Cu-RGO-IONP-PEG. The stability of ^{64}Cu-RGO-IONP-PEG was examined in mouse serum for 72 h at 25 °C with slight shaking. In addition, these nanoparticles have been previously characterized by UV–Vis absorbance, ultra-transmission electron microscopy (ultra-TEM), and X-ray photoelectron (XPS) [21].

2.3. Murine model of hindlimb ischemia

All animal studies were conducted under a protocol approved by the University of Wisconsin Institutional Animal Care and Use Committee. Right unilateral hindlimb ischemia was induced in six-week-old female BALB/c mice (Harlan, Indianapolis, IN) as previously described [22]. In summary, animals were anesthetized with 2% isoflurane before the femoral triangle was exposed by a modified oblique incision at mid-abdominal level. The left femoral artery was separated from the femoral vein and nerve by blunt dissection distal to the inguinal ligament. The artery was tied proximally and distally with a 6/0 nylon suture (AROSurgical Corp., Newport Beach, CA) and cut between the two sutures. A sham procedure was performed on the contralateral hindlimb to serve as the internal control. Of note, the reason for placing the incision at the mid-abdominal level was to eliminate the possibility of superposition of radioactivity signals from a surgical wound and the ischemic muscle tissue.

2.4. Laser Doppler imaging of hindlimb ischemia

Three mice from each group were used for serial laser Doppler imaging studies. Baseline laser Doppler images were obtained before surgery and soon after surgery with a laser Doppler imaging system (moorLDI2-HR, Moor Instruments, DE, USA).

2.5. ^{64}Cu labeling of RGO-IONP-PEG

^{64}Cu was produced via a ^{64}Ni(p,n)^{64}Cu reaction using a CTI RDS 112 cyclotron at the University of Wisconsin – Madison, as described previously [23]. For a typical radiolabeling, $^{64}CuCl_2$ (74–148 MBq) was diluted in 300 μL of 0.1 M sodium acetate buffer (pH = 6.5) and added to 200 μL of RGO-IONP-PEG. The reaction was allowed to proceed at 37 °C for 30 min with constant stirring. ^{64}Cu-RGO-IONP-PEG was purified using PD-10 columns with PBS as the mobile phase.

2.6. PET imaging and analysis

PET scans were performed using a microPET/microCT Inveon rodent model scanner (Siemens Medical Solutions USA, Inc.). Procedures for image acquisition and reconstruction and region-of-interest (ROI) analysis of the PET data were described previously [24]. Quantitative PET data were presented as %ID/g. Hindlimb ischemia model mice received an intravenous injection of ~10 MBq of ^{64}Cu-RGO-IONP-PEG via tail vein before serial PET scans.

2.7. Ex vivo biodistribution study

After the last PET scans, biodistribution studies were carried out to confirm that the %ID/g values based on PET imaging truly represented the radioactivity distribution in the hindlimb ischemia model. Mice were euthanized, and blood, ischemic/non-ischemic muscle and major organs/tissues were collected and wet-weighed. The radioactivity in the tissue was measured using a gamma counter (PerkinElmer, USA) and presented as %ID/g (mean ± SD).

2.8. Histological staining of tissues

All images were acquired with a Nikon Eclipse Ti microscope (Melville, NY, USA). Tissues were provided to the University of Wisconsin Carbone Cancer Center Experimental Pathology Laboratory for processing and sectioning. Frozen tissue slices of 5 μm were fixed with cold acetone and stained using the Iron Staining Kit (Sigma-Aldrich, St. Louis, MO, USA) containing potassium ferrocyanide solution and hydrochloric acid. Slides were placed in cold acetone for 15 min and air dried for 15 min at room temperature. Slides were immersed in a mixture of 1:1 potassium ferrocyanide and hydrochloric acid solution for 10 min and removed. Next, slides were washed five times with tap water before counterstaining with

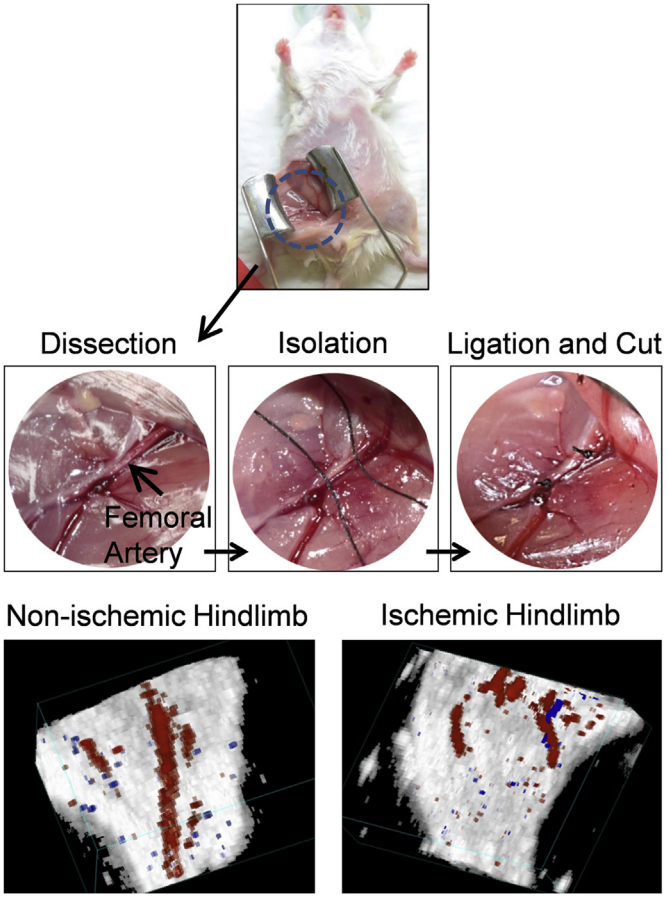

Fig. 1. The murine model of hindlimb ischemia was used as a representative model of peripheral arterial disease (PAD). Mice were anesthetized, and an incision was made at the mid-abdominal level. The femoral artery was isolated, ligated, and cut to produce the ischemic model. Doppler ultrasound imaging confirmed the success of the surgery, showing significantly diminished blood flow in the ischemic hindlimb.

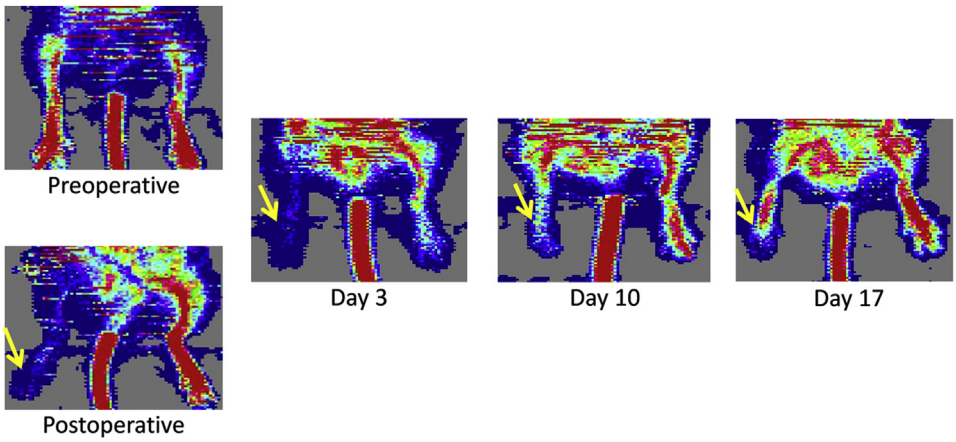

Fig. 2. Serial laser Doppler imaging shows the change of blood perfusion in the ischemic hindlimb after surgical ligation of the femoral artery. The ischemic hindlimb gradually recovers over time, and blood flow normalizes by 17 days post-surgery. The yellow arrows denote the ischemic hindlimbs. (For interpretation of the references to colour in this figure legend, the reader is referred to the web version of this article.).

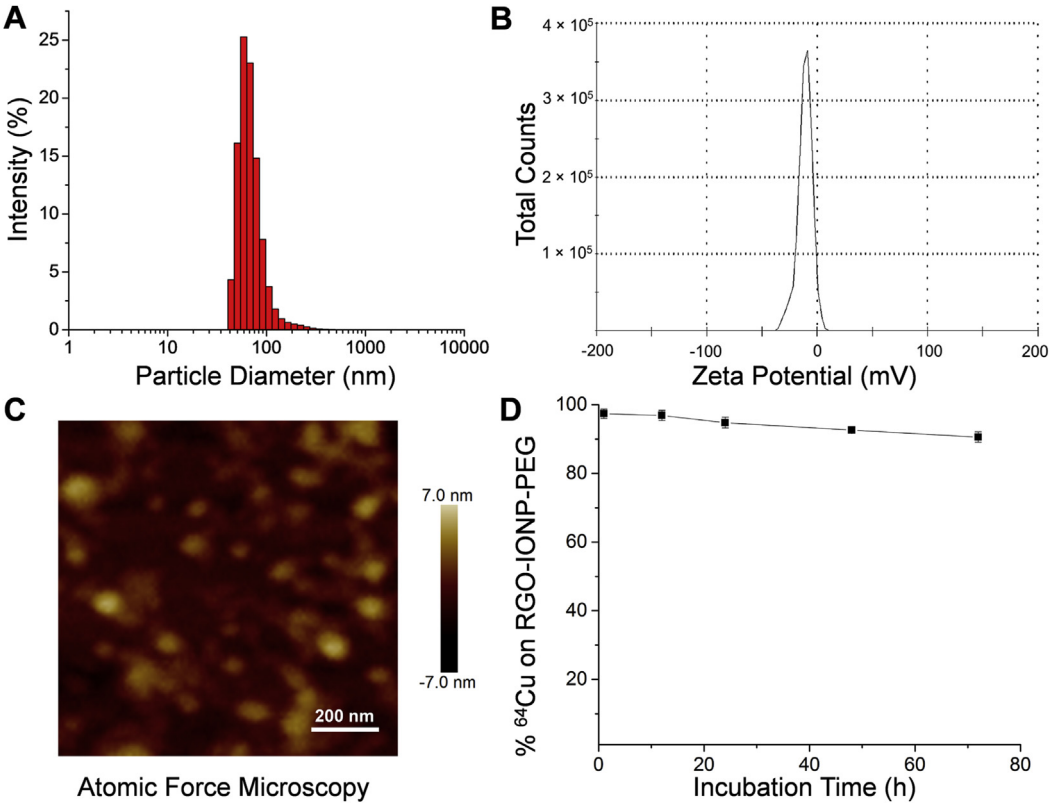

Fig. 3. ^{64}Cu-RGO-IONP-PEG were characterized by size, surface charge, morphology, and serum stability. A. The hydrodynamic diameter of nanoparticles was determined by DLS and shown to be 68.2 ± 7.4 nm with a polydispersion index (PDI) value of 0.3. B. The surface charge was determined by zeta potential analysis and found to be −11.0 ± 6.6 mV. C. The morphology of nanoparticles was examined using AFM, allowing for confirmation of nanoparticle size and shape. D. Nanoparticle stability was examined by incubation in mouse serum. In serum, 90.6 ± 1.5% of nanoparticles remained stable at 72 h.

eosin. Slides were incubated in eosin for 30 s, and washed five times with deionized water, followed by two washes with 90, 95, and 100% ethanol. Slides were allowed to dry at room temperature before being receiving a coverslip.

2.9. Photoacoustic imaging

The Vevo LAZR Photoacoustic Imaging System (VisualSonics, Inc., Toronto, Canada) with a laser excitation wavelength of 808-nm and a focal depth of 100 mm was used to acquire photoacoustic and ultrasound images of the ischemic hindlimb and non-ischemic hindlimb pre- and post-injection of ^{64}Cu-RGO-IONP-PEG. In addition to photoacoustic imaging, this system produced high-resolution Doppler ultrasound images of the hindlimb to evaluate vasculature.

2.10. Statistical analysis

Quantitative data were expressed as mean ± S.D. Means of two groups were compared using the Student *t*-test. *P* values < 0.05

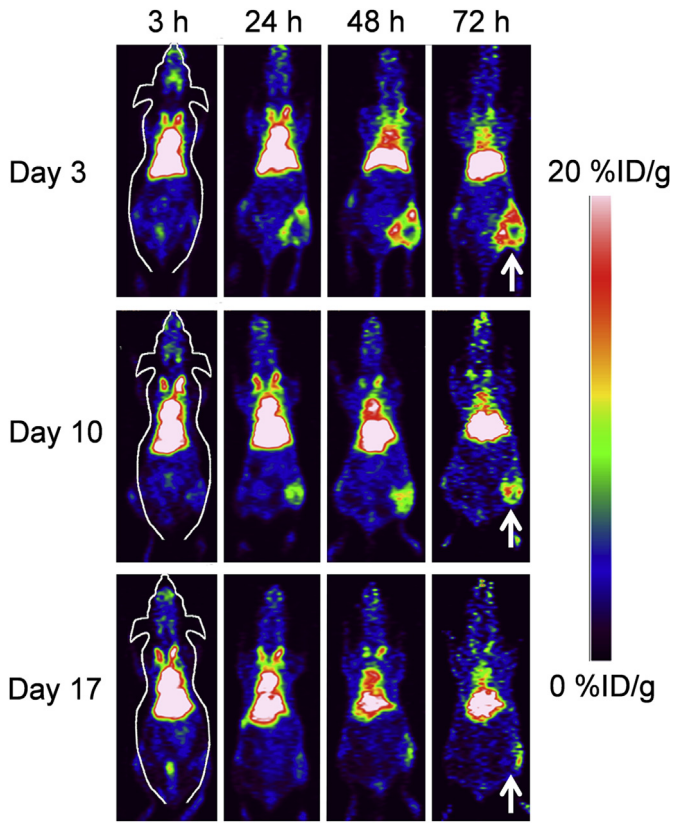

Fig. 4. PET imaging was performed 3, 10, and 17 days after surgically-induced hindlimb ischemia. PET images of mice were acquired from 3 h to 72 h post-injection of nanoparticles, and representative coronal sections of PET images show enhanced uptake of ^{64}Cu-RGO-IONP-PEG during initial disease stages, with less passive accumulation once the blood flow begins to normalize by Day 17. The white arrows denote the ischemic hindlimb.

were considered statistically significant.

3. Results and discussion

A few studies have examined the efficacy of nanoparticle-based therapy in hindlimb ischemia, as a representative murine model of PAD, but the accumulation of nanoparticles has not well assessed quantitatively, which is mandatory for successful nanoparticle-based therapy. Also, nanoparticle accumulation via the EPR effect in PAD has been suggested, but not been evaluated sequentially and quantitatively [15]. As RGO-IONP-PEG displays a long circulation half-life *in vivo*, it is an excellent candidate for molecular imaging and drug delivery [21,25]. In addition, this versatile nanoparticle has been employed for a wide range of imaging modalities, including MRI, PET, SPECT, and photoacoustic imaging [21]. Besides acting as a contrast agent for imaging, RGO-IONP-PEG can successfully carry large payloads of drug and may produce heat through photothermal therapy [25]. While RGO-IONP-PEG has been investigated in cancer models, they have not been utilized for imaging of hindlimb ischemia.

Our previous study showed that the ischemic hindlimb will start to heal around 20–30 days after surgical ligation of the femoral artery [26]. In the hindlimb ischemia model, angiogenesis is highest during the time points after the surgery [27]. Since the EPR effect results from the abnormally permeable vasculature [28], we expected that nanoparticle localization would be highest during initial disease stages and would diminish as the vasculature normalized. The first group of mice was administered ^{64}Cu-RGO-IONP-PEG at 3 days post-surgery and imaged for 72 h using PET. The second group of mice received an injection of nanoparticles at 10 days post-surgery, and the third group received the nanoparticle injection 17 days after surgery. Consistent with the first group, PET imaging was performed to map the distribution and localization of nanoparticles in the ischemic hindlimb for 72 h after injection. After the last time point, mice were euthanized, and biodistribution studies were performed to validate the PET results.

Surgical induction of ischemia was accomplished through ligation of the femoral artery, which provides a simplified approach with minimal complications [29]. With the mouse placed in supine position, an incision was made on the mid-abdominal level (Fig. 1). Retractors were used to open the wound, allowing for enhanced visualization. The femoral vein was separated from the femoral artery before ligation and cutting of the femoral artery. Laser Doppler images confirmed the success of the model post-surgery with the surgical hindlimb showing significantly diminished blood flow (Fig. 1). In addition, high-resolution Doppler ultrasound images showed the arterial blood flow in both hindlimbs, with the non-ischemic hindlimb showing the femoral artery while the ischemic hindlimb displayed an abrupt cut of the femoral artery.

Serial laser Doppler images were obtained to show the changes in blood perfusion pre- and post-surgery (Fig. 2). Before surgical ligation of the femoral artery, blood perfusion is high (red) in both hindlimbs. Blood perfusion significantly diminishes after surgery in the surgical hindlimb, while the non-surgical hindlimb showed no changes in blood perfusion. Serial Doppler imaging was performed to monitor the changes in blood flow over time. Blood perfusion was significantly diminished at 3 and 10 days post-surgery, yet the vasculature of the surgical hindlimb showed significant improvements in blood flow by 17 days post-surgery.

RGO-IONPs were synthesized using procedures described previously [21]. For optimal stability and increased circulation time, the nanoparticles were functionalized with two layers of polyethylene glycol (PEG). After synthesis, ^{64}Cu-RGO-IONP-PEG were characterized to ensure their identity and proper modifications. These nanoparticles were characterized previously using UV–Vis absorbance, transmission electron microscopy (TEM), and X-ray photoelectron (XPS) [21]. In this study, the hydrodynamic diameter was determined by dynamic light scattering (DLS), the surface charge was ascertained through zeta potential analysis, and morphology of the nanoparticles was confirmed by atomic force microscopy (AFM) (Fig. 3). As shown in Fig. 3A, the size of ^{64}Cu-RGO-IONP-PEG was found to be 68.2 ± 7.4 nm. A representative histogram has been provided. The surface charge of this nanoplatform was determined to be −11.0 ± 6.6 mV (Fig. 3B). AFM confirmed the size and homogeneity of the nanoparticles (Fig. 3C). To determine the radiostability, ^{64}Cu-RGO-IONP-PEG were incubated in mouse serum for 40 h. Nanoparticles remained stable with >96% of the nanoparticles remaining ^{64}Cu-bound after 24 h. At the final time point (72 h), 90.6 ± 1.5% of nanoparticles were found to be stable, thus confirming the enhanced stability of ^{64}Cu-RGO-IONP-PEG in mouse serum (Fig. 3D).

PET imaging was started at 3 h and continued through 72 h post-injection of nanoparticles (Fig. 4). Accumulation of ^{64}Cu-RGO-IONP-PEG was evident at 24 h in each group (Day 3, Day 10, and Day 17) and increased through 72 h post-injection, with the highest uptake displayed at 72 h post-injection. Coronal sections of PET scans show differential uptake between each group at 48 h and 72 h post-injection. Mice that received the nanoparticle injection 3 days after surgery (Day 3) displayed the highest accumulation of ^{64}Cu-RGO-IONP-PEG, whereas fewer nanoparticles were able to accumulate passively in the ischemic hindlimb of Day 10 and Day 17 groups at 72 h post-injection. This confirmed our hypothesis that

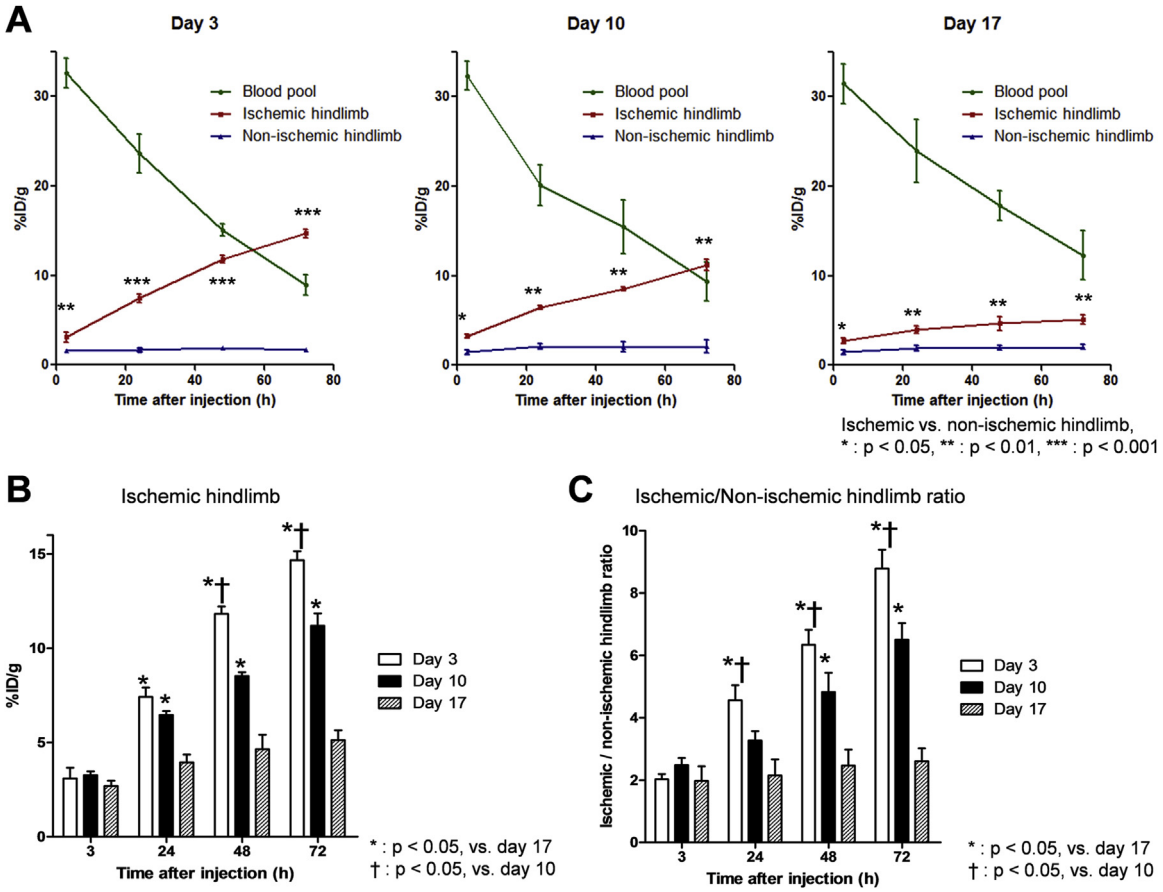

Fig. 5. Analysis of PET data to determine %ID/g values of ^{64}Cu-RGO-IONP-PEG in the ischemic hindlimb, non-ischemic hindlimb, and blood pool. A. The concentration of nanoparticle was similar in each group at 3 h post-injection and remained similar at the final time point (72 h). Accumulation of nanoparticles was lowest at 3 h post-injection and increased with time. Each group (Day 3, 10, and 17) showed statistically significant differences in nanoparticle accumulation between the ischemic and non-ischemic hindlimb. B. The %ID/g of ^{64}Cu-RGO-IONP-PEG in the ischemic hindlimb was highest at 3 days post-surgery and lowest at day 17. C. The ratio of ischemic to non-ischemic hindlimb %ID/g showed statistically significance differences between %ID/g at 24, 48, and 72 h post injection for each group of mice.

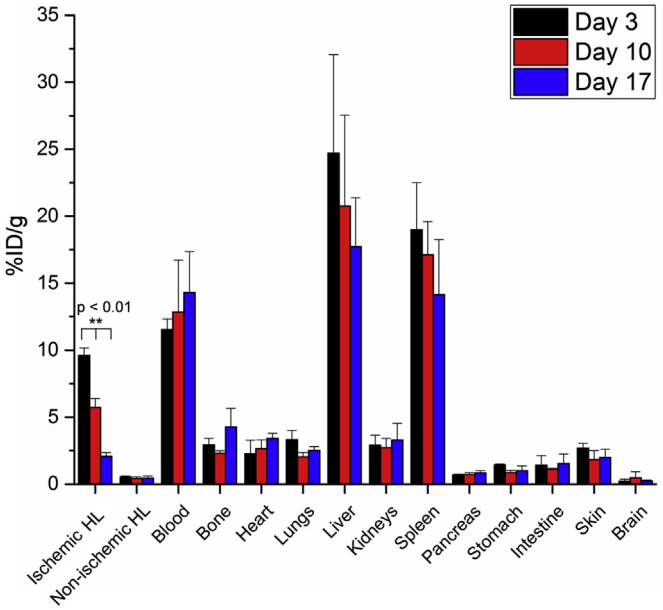

Fig. 6. Biodistribution studies at 72 h post-injection confirm that uptake of ^{64}Cu-RGO-IONP-PEG in the ischemic hindlimb was highest at 3 days post-surgery and lowest at 17 days post-surgery. The concentration of nanoparticle in the blood pool corroborated positron emission tomography (PET) findings and %ID/g values in other organs and tissues were within expected ranges. HL: hindlimb.

nanoparticle accumulation was dependent upon the extent of ischemia in the hindlimb.

The accumulation of ^{64}Cu-RGO-IONP-PEG in ischemic tissue was diminished at the delayed time points in the present study. While the EPR effect in the ischemic hindlimb is thought to be caused by angiogenesis, the time course of angiogenesis has been well evaluated by gene expression analysis [27], and also by *in vivo* imaging using radiolabeled probes [26,30]. Lee *et al.* reported that genes related to angiogenesis are overexpressed until 7 days post-surgery [27]. Orbay *et al.* showed that ^{64}Cu-NOTA-TRC105, targeting CD105 (i.e. endoglin, which is abundantly expressed in angiogenic endothelial cells), localized in the ischemic hindlimb highest 3 days post-surgery and lowest at 24 days post-surgery [26]. Similarly, Willmann *et al.* employed vascular endothelial growth factor-121 (VEGF-121) for targeting of vascular endothelial growth factor receptor (VEGF-R), which is an angiogenic marker [30]. Also, radiolabeled VEGF121 accumulated highest at 8 days post-surgery and uptake was lowest at 29 days post-surgery. Based on the results of the previous reports, we could confirm that the time course of angiogenesis and accumulation of ^{64}Cu-RGO-IONP-PEG in the present study are well correlated, which further confirms the time course of the EPR effect in the murine model of hindlimb ischemia.

Quantitative assessment of the PET data provided a direct comparison between nanoparticle uptake in the blood pool, non-ischemic hindlimb, and ischemic hindlimb (Fig. 5). At 3 h post-injection, the concentration of ^{64}Cu-RGO-IONP-PEG in the blood

pool was found to be similar at ~30%ID/g (Fig. 5A). In addition, ^{64}Cu-RGO-IONP-PEG was removed from circulation at similar rates, shown by the linear decrease in blood pool %ID/g. This suggests several things, including that each nanoparticle injection displayed similar stability, disease stage did not affect the circulation of the nanoparticles, and removal of the nanoparticle from circulation was concentration-independent (i.e. zero-order kinetics [31]). By 72 h post-injection, ~10% of ^{64}Cu-RGO-IONP-PEG remained in the blood pool, which was later confirmed by biodistribution analysis. Accumulation of ^{64}Cu-RGO-IONP-PEG was determined in other organs and tissues, and these results have provided in the Supplementary Information (Tables S1–3).

Data showed differential uptake of ^{64}Cu-RGO-IONP-PEG in the ischemic and non-ischemic in each group (Day 3, 10, and 17). As hypothesized, this difference was highest at Day 3 and lowest at Day 17, suggesting that nanoparticle accumulation was dependent upon the degree of ischemia in the hindlimb (Fig. 5A, B). The accumulation of ^{64}Cu-RGO-IONP-PEG was highest at 72 h post-injection for each group of mice, with values of 14.68 ± 0.48, 11.2 ± 0.65, and 5.1 ± 0.53%ID/g for Day 3, Day 10, and Day 17, respectively (Fig. 5B). The amount of nanoparticle accumulated negatively correlated with the perfusion of the ischemic hindlimb (Figs. 2 and 5). For comparison, the ratios of ischemic to non-ischemic hindlimb %ID/g were examined and showed a statistically significant difference in nanoparticle uptake between the groups at 48 h and 72 h post-injection (Fig. 5C).

Ex vivo biodistribution studies were performed to confirm the PET findings (Fig. 6). Similar to PET analysis, biodistribution showed the liver and spleen having the highest uptake of nanoparticles. Both PET and biodistribution studies agreed that nanoparticle accumulation in the blood at 72 h post-injection was ~10%ID/g. Interestingly, biodistribution studies revealed a slight difference in the uptake of nanoparticles in the ischemic hindlimb, yet statistically significant differences in nanoparticle uptake were found between the three groups (Day 3, 10, and 17). The lower %ID/g found in biodistribution studies were determined to be related to the tissue procurement process. In an attempt to ensure that all ischemic tissue was removed for biodistribution studies, we expected that some normal muscle may have been obtained as well, leading to slight decreases in %ID/g.

A limitation of PET is that it only detects the radioisotopes, not the nanoparticles. Using the intrinsic photoacoustic imaging property and *ex vivo* histology study, we further confirmed the uptake of nanoparticles in the surgery hindlimb. While RGO-IONPs have been extensively examined for MRI purposes, few studies have employed photoacoustic imaging for mapping of these nanoparticles *in vivo* [21]. As RGO-IONPs absorb light in the near-infrared region (NIR), photoacoustic imaging was performed by exciting the nanoparticles with an 808-nm laser (Fig. 7). First, the nanoparticles were characterized for their potential use as photoacoustic imaging agents. This was accomplished through phantom imaging with different concentrations of RGO-IONP to determine the lower PA signal detection limit (Fig. S1). The ischemic and non-ischemic hindlimbs of mice were imaged before (Fig. 7A) and 72 h after (Fig. 7B) receiving a single bolus injection of ^{64}Cu-RGO-IONP-PEG. Photoacoustic imaging utilizes ultrasound waves for visualizing the legs (brightness mode, B-mode), while the photoacoustic transducers and excitation lasers work together to produce a photoacoustic image (photoacoustic mode, PA-mode). In this case, the fused image combines the anatomical characteristics of the hindlimb with the corresponding photoacoustic signal. The highest photoacoustic signal was found in the ischemic hindlimb, with minimal background signal found in the pre-injected hindlimb. While endogenous molecules such as hemoglobin and melanin can produce intrinsic PA signal, pre-injection imaging was performed as a control [32,33]. Additionally, we found positive PA signal in liver sections of mice after receiving an injection of nanoparticles at 3 days post-surgery (Fig. S2). This further corroborated our findings from PET imaging and confirmed that RGO-IONP is a suitable construct for photoacoustic imaging.

Multimodality imaging agents make it feasible to confirm initial or atypical findings. While PET imaging is highly quantitative, the acquired images are only depictions of the isotope and not the actual imaging probe. For this reason, PET imaging will show uptake of the free isotope, or isotope that has become unattached from the nanoparticle. While this does not significantly

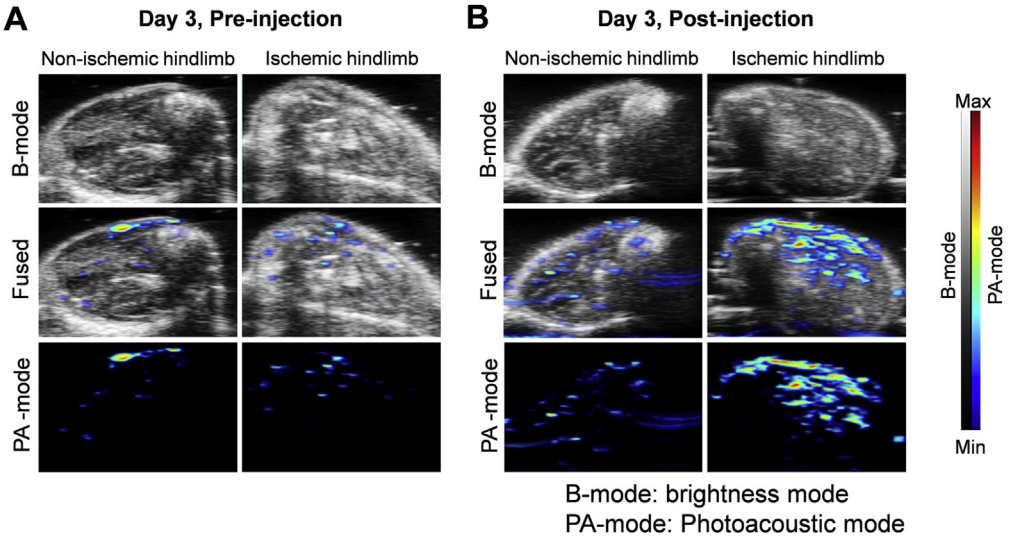

Fig. 7. Photoacoustic imaging of hindlimb ischemia pre- and post-intravenous injection of ^{64}Cu-RGO-IONP-PEG. Photoacoustic imaging combines the anatomical information of ultrasound imaging (B-mode) with the photoacoustic signal (PA-mode) to produce a fused image. Enhanced PA signal signifies the presence of nanoparticles in the ischemic tissue. A. The hindlimb of mice imaged before nanoparticle injection displayed minimal background signal. B. Photoacoustic signal was highest in the ischemic hindlimb after receiving an intravenous bolus injection of nanoparticles. For comparison, there was minimal uptake in the non-ischemic hindlimb post-injection.

affect imaging with ^{64}Cu, other isotopes have been shown to localize in specific organs or tissues in the body (e.g. Zirconium-89 accumulates in the bone [34]). This does not hold true for photoacoustic imaging, as this technique images the nanoparticles directly, thus confirming the uptake and distribution found by PET imaging.

Ex vivo staining of tissue with Prussian blue allowed for visualization of iron content (Figs. S3 and S4). The Prussian blue stain is based on the conversion of Fe^{2+} to Fe^{3+} in forming $Fe_4(Fe[CN]_6)_3$, which results in a bright blue color [35]. The ischemic and non-ischemic hindlimb tissues of mice from Day 3 group were excised for histological analysis. Tissue sections were stained with Prussian blue and a counterstain (eosin) before analysis. In the ischemic hindlimb, positive blue staining indicates the presence of iron. There was little blue stain observed in the control (non-ischemic) hindlimb, suggesting little uptake of nanoparticles in the non-ischemic hindlimb, similar to PET and photoacoustic findings. In addition, the ischemic muscle tissue sections were stained before and after injection to further validate the presence of nanoparticles.

Future studies employing nanoparticles for molecular imaging for PAD may find more suitable nanoconstructs. As this study relied upon the passive accumulation of RGO-IONPs via the EPR effect, we would expect that active targeting of these nanoparticles could enhance the localization in ischemic tissues. Previously, we investigated the biosafety of RGO-IONP-PEG *in vitro* and *in vivo* and found no signs of toxicity; thus, RGO-IONP-PEG may be a viable nanoplatform for future clinical applications [21]. Furthermore, examination of the potential use of theranostics may provide information for allowing image-guided drug delivery for PAD. Previously, Nagahama *et al.* examined the treatment of neovascularization using pioglitazone-loaded nanoparticles in a murine model of hindlimb ischemia [36]. Similarly, it was shown that p-hydroxy benzyl alcohol significantly increased blood flow perfusion and angiogenesis in murine models of hindlimb ischemia, thus widening the field of potential therapies for PAD [37].

4. Conclusions

In summary, our study suggests that EPR-mediated accumulation of ^{64}Cu-RGO-IONP-PEG allows for multimodality of imaging of PAD, shown by using a murine hindlimb ischemia model. It was revealed that nanoparticle accumulation was dependent upon the extent of ischemia, as a high degree of angiogenesis resulted in EPR-mediated nanoparticle localization. As RGO-IONPs display physiochemical characteristics suitable for multimodality imaging and therapy, these nanoparticles may potentially show clinical relevance as theranostic agents, leading to more effective strategies for disease treatment and monitoring.

Author contributions

C.G.E, H.J.I., F.C., and W.C. conceived, designed and oversaw all of the studies; C.G.E, H.J.I., L.F., S.A.G., R.H., H.O., and C.X. performed the experiments; S.Y.C., R.J.N., Z.L., D.S.L, and W.C. reviewed the data and provided input; C.G.E., H.J.I., and W.C. wrote the paper, which all authors edited.

Disclosure

The authors declare that they have no competing interests.

Acknowledgements

Funding: This work was supported, in part, by the University of Wisconsin – Madison, the National Institutes of Health (NIBIB/NCI 1R01CA169365, P30CA014520, 5T32GM08349, T32CA009206), the National Science Foundation (DGE-1256259), and the American Cancer Society (125246-RSG-13-099-01-CCE).

Appendix A. Supplementary data

Supplementary data related to this article can be found at http://dx.doi.org/10.1016/j.biomaterials.2016.05.018.

References

[1] K. Yang, L. Feng, H. Hong, W. Cai, Z. Liu, Preparation and functionalization of graphene nanocomposites for biomedical applications, Nat. Protoc. 8 (2013) 2392–2403.
[2] H. Hong, Y. Zhang, J.W. Engle, T.R. Nayak, C.P. Theuer, R.J. Nickles, et al., In vivo targeting and positron emission tomography imaging of tumor vasculature with (66)Ga-labeled nano-graphene, Biomaterials 33 (2012) 4147–4156.
[3] P. Abdulhannan, D.A. Russell, S. Homer-Vanniasinkam, Peripheral arterial disease: a literature review, Br. Med. Bull. 104 (2012) 21–39.
[4] B.G. Samolsky Dekel, R.M. Melotti, M. Gargiulo, A. Freyrie, A. Stella, G. Di Nino, Pain management in peripheral arterial obstructive disease: oral slow-release oxycodone versus epidural l-bupivacaine, Eur. J. Vasc. Endovasc. Surg. 39 (2010) 774–778.
[5] A. American Diabetes, Peripheral arterial disease in people with diabetes, Diabetes Care 26 (2003) 3333–3341.
[6] T.F. Luscher, M.A. Creager, J.A. Beckman, F. Cosentino, Diabetes and vascular disease: pathophysiology, clinical consequences, and medical therapy: part II, Circulation 108 (2003) 1655–1661.
[7] V.N. Varu, M.E. Hogg, M.R. Kibbe, Critical limb ischemia, J. Vasc. Surg. 51 (2010) 230–241.
[8] J.S. Berger, W.R. Hiatt, Medical therapy in peripheral artery disease, Circulation 126 (2012) 491–500.
[9] J. Tongers, J.G. Roncalli, D.W. Losordo, Therapeutic angiogenesis for critical limb ischemia: microvascular therapies coming of age, Circulation 118 (2008) 9–16.
[10] B.G. Amsden, Delivery approaches for angiogenic growth factors in the treatment of ischemic conditions, Expert Opin. Drug Deliv. 8 (2011) 873–890.
[11] C. Tu, S. Das, A.B. Baker, J. Zoldan, L.J. Suggs, Nanoscale strategies: treatment for peripheral vascular disease and critical limb ischemia, ACS Nano 9 (2015) 3436–3452.
[12] A.W. Pollak, P.T. Norton, C.M. Kramer, Multimodality imaging of lower extremity peripheral arterial disease: current role and future directions, Circ. Cardiovasc. Imaging 5 (2012) 797–807.
[13] A.R. Owen, G.H. Roditi, Peripheral arterial disease: the evolving role of non-invasive imaging, Postgrad. Med. J. 87 (2011) 189–198.
[14] S.C. Josephs, H.A. Rowley, G.D. Rubin, G. American Heart Association Writing, Atherosclerotic peripheral vascular disease symposium II: vascular magnetic resonance and computed tomographic imaging, Circulation 118 (2008) 2837–2844.
[15] J. Kim, L. Cao, D. Shvartsman, E.A. Silva, D.J. Mooney, Targeted delivery of nanoparticles to ischemic muscle for imaging and therapeutic angiogenesis, Nano Lett. 11 (2011) 694–700.
[16] J. Zhang, G. Wang, D. Mao, A.T. Han, N.N. Xiao, X. Qi, et al., Targeted in vivo imaging of mouse hindlimb ischemia using fluorescent gelatin nanoparticles, J. Nanomater. 2015 (2015) 7.
[17] M.R. Stacy, W. Zhou, A.J. Sinusas, Radiotracer imaging of peripheral vascular disease, J. Nucl. Med. 54 (2013) 2104–2110.
[18] T.K. Lee, H. Hwang, K.S. Na, J. Kwon, H.S. Jeong, P. Oh, et al., Effect of angiogenesis induced by consecutive intramuscular injections of vascular endothelial growth factor in a hindlimb ischemic mouse model, Nucl. Med. Mol. Imaging 48 (2014) 225–229.
[19] H. Kobayashi, R. Watanabe, P.L. Choyke, Improving conventional enhanced permeability and retention (epr) effects; what is the appropriate target? Theranostics 4 (2013) 81–89.
[20] H. Niiyama, N.F. Huang, M.D. Rollins, J.P. Cooke, Murine model of hindlimb ischemia, J. Vis. Exp. (2009) 1035.
[21] K. Yang, L. Hu, X. Ma, S. Ye, L. Cheng, X. Shi, et al., Multimodal imaging guided photothermal therapy using functionalized graphene nanosheets anchored with magnetic nanoparticles, Adv. Mater. 24 (2012) 1868–1872.
[22] H. Orbay, H. Hong, Y. Zhang, W. Cai, Pet/spect imaging of hindlimb ischemia: focusing on angiogenesis and blood flow, Angiogenesis 16 (2013) 279–287.
[23] S. Shi, H. Orbay, Y. Yang, S.A. Graves, T.R. Nayak, H. Hong, et al., Pet imaging of abdominal aortic aneurysm with 64cu-labeled anti-cd105 antibody fab fragment, J. Nucl. Med. 56 (2015) 927–932.
[24] Y. Yang, R. Hernandez, J. Rao, L. Yin, Y. Qu, J. Wu, et al., Targeting cd146 with a 64cu-labeled antibody enables in vivo immunopet imaging of high-grade

gliomas, Proc. Natl. Acad. Sci. U. S. A. 112 (2015) E6525–E6534.
[25] Y.Q. Yang, A.M. Asiri, Z.W. Tang, D. Du, Y.H. Lin, Graphene based materials for biomedical applications, Mater. Today 16 (2013) 365–373.
[26] H. Orbay, Y. Zhang, H. Hong, T.A. Hacker, H.F. Valdovinos, J.A. Zagzebski, et al., Positron emission tomography imaging of angiogenesis in a murine hindlimb ischemia model with 64cu-labeled trc105, Mol. Pharm. 10 (2013) 2749–2756.
[27] C.W. Lee, E. Stabile, T. Kinnaird, M. Shou, J.M. Devaney, S.E. Epstein, et al., Temporal patterns of gene expression after acute hindlimb ischemia in mice: insights into the genomic program for collateral vessel development, J. Am. Coll. Cardiol. 43 (2004) 474–482.
[28] K. Greish, Enhanced permeability and retention (epr) effect for anticancer nanomedicine drug targeting, Methods Mol. Biol. 624 (2010) 25–37.
[29] D.P. Slovut, E.C. Lipsitz, Surgical technique and peripheral artery disease, Circulation 126 (2012) 1127–1138.
[30] J.K. Willmann, K. Chen, H. Wang, R. Paulmurugan, M. Rollins, W. Cai, et al., Monitoring of the biological response to murine hindlimb ischemia with 64cu-labeled vascular endothelial growth factor-121 positron emission tomography, Circulation 117 (2008) 915–922.
[31] M.T. Zhu, W.Y. Feng, Y. Wang, B. Wang, M. Wang, H. Ouyang, et al., Particokinetics and extrapulmonary translocation of intratracheally instilled ferric oxide nanoparticles in rats and the potential health risk assessment, Toxicol. Sci. 107 (2009) 342–351.
[32] A.M. Yashchenok, J. Jose, P. Trochet, G.B. Sukhorukov, D.A. Gorin, Multifunctional polyelectrolyte microcapsules as a contrast agent for photoacoustic imaging in blood, J. Biophot. (2016) n/a-n/a. [Epub ahead of print].
[33] G.C. Langhout, D.J. Grootendorst, O.E. Nieweg, M.W. Wouters, J.A. van der Hage, J. Jose, et al., Detection of melanoma metastases in resected human lymph nodes by noninvasive multispectral photoacoustic imaging, Int. J. Biomed. Imaging 2014 (2014) 163652.
[34] D.S. Abou, T. Ku, P.M. Smith-Jones, In vivo biodistribution and accumulation of 89zr in mice, Nucl. Med. Biol. 38 (2011) 675–681.
[35] T. Schlorf, M. Meincke, E. Kossel, C.C. Gluer, O. Jansen, R. Mentlein, Biological properties of iron oxide nanoparticles for cellular and molecular magnetic resonance imaging, Int. J. Mol. Sci. 12 (2010) 12–23.
[36] R. Nagahama, T. Matoba, K. Nakano, S. Kim-Mitsuyama, K. Sunagawa, K. Egashira, Nanoparticle-mediated delivery of pioglitazone enhances therapeutic neovascularization in a murine model of hindlimb ischemia, Arterioscler. Thromb. Vasc. Biol. 32 (2012) 2427–2434.
[37] B.R. Cho, D.R. Ryu, K.S. Lee, D.K. Lee, S. Bae, D.G. Kang, et al., P-hydroxybenzyl alcohol-containing biodegradable nanoparticle improves functional blood flow through angiogenesis in a mouse model of hindlimb ischemia, Biomaterials 53 (2015) 679–687.